RSC Advances

PAPER

View Article Online
View Journal | View Issue

Cite this: *RSC Adv.*, 2016, **6**, 98632

Solution-grown GeO_2 nanoparticles with a nearly 100% yield as lithium-ion battery anodes†

Guo-An Li, Wei-Chin Li, Wei-Chung Chang and Hsing-Yu Tuan*

Received 10th August 2016
Accepted 9th October 2016

DOI: 10.1039/c6ra20171g

www.rsc.org/advances

Germanium oxide (GeO_2) nanoparticles were synthesized with a nearly 100% production yield in a nonionic reverse micelle system at ambient temperature. The procedure is a facile and energy saving strategy for producing germanium oxide nanoparticles with ultra large throughput. As-prepared GeO_2 nanoparticles can be directly used as anode materials without any post-treatment or other supplementary additives for lithium ion batteries. GeO_2-anodes exhibited good electrochemical performance in terms of both gravimetric and volumetric capacity. The GeO_2 anodes have a reversible capacity of approximately 1050 mA h g^{-1} at a rate of 0.1C, close to its theoretical capacity (1100 mA h g^{-1}), and good rate capability without severe capacity decade. The volumetric capacity of the GeO_2 anodes reaches 660 mA h cm^{-3}, which is higher than the performance of commercial graphite anode (370–500 mA h cm^{-3}). Coin type and pouch type full cells assembled for electronic devices applications were also demonstrated. A single battery is shown to power LED array over 120 bulbs with a driving current of 650 mA. Based on the above, the micelle process of GeO_2 nanoparticle synthesis provides a possible solution to high-capacity nanoparticles' scalable manufacturing for lithium ion battery applications.

Introduction

Lithium-ion batteries (LIBs), as a state-of-the-art technology in energy storage devices, have been utilized in a wide range of applications due to their relatively high energy density, long cycle life span, and good rate capability, *etc.*[1–4] Ge-based materials have been intensively studied due to their remarkable high capacities over 1000 mA h g^{-1} as anode materials for LIBs owing to Li–Ge alloying mechanism.[5–8] For example, germanium has a high capacity of 1384 mA h g^{-1}, which is much higher than the theoretical capacity of commercial graphite (372 mA h g^{-1}).[9,10] Nevertheless, two challenging problems of Ge-based material must be addressed. One is Ge's huge volume change (~370%) during charging and discharging procedures which induces active material cracking and fracture and produces fresh surface that consumes lithium and causes irreversibility capacity loss. Recent development of a variety of Ge nanostructures is a highly effective strategy to improve the negative influence of electrode's volume expansion on battery performance.[11–15] On the other hand, the other critical problem is that the limitation of Ge's high cost and expensive manufacturing process, but this issue is rarely addressed.[16]

Germanium dioxide, also called germania, is much less expensive than germanium, and widely used in optical fibers, polymer catalysts, and also as a component of waveguides where it is capability of modulating the index of refraction.[17,18] In general, various metal oxide nanostructures exhibit excellent electrochemical performance in lithium-ion batteries.[19–22] GeO_2 reacts with lithium ion and transforms irreversibly into germanium nanoparticles and Li_2O matrix during beginning of reduction process, and then germanium nanoparticles react reversibly with lithium ion through alloying mechanism for the following lithiation/delithiation process.[23,24]

$$GeO_2 + 4Li \rightarrow Ge + 2Li_2O$$

$$Ge + 4.4Li \leftrightarrow Li_{4.4}Ge$$

Based on the above reaction, GeO_2 has a theoretical capacity of 1100 mA h g^{-1} (4653 mA h cm^{-3}) which is comparable to germanium's performance. However, the practical capacity of GeO_2 is not well-maintained. The rapid capacity loss of the GeO_2 electrode fabricated by Brousse *et al.*[25] dropped from 740 to 225 mA h g^{-1} after 10 cycles is attributed to the ~230% volume change during electrochemical test. Recently, lots of efforts have been made to address situations to obtain progressive improvement. GeO_2 electrode maintains cycling stability with the aid of carbonaceous additives to form composites, which effectively alleviate the stress from volume variation during lithium intake/removal.[26–30] In the meanwhile, supplementary additives offer additional electron transfer pathway, which

Department of Chemical Engineering, National Tsing Hua University, 101, Section 2, Kuang-Fu Road, Hsinchu, Taiwan 30013, Republic of China. E-mail: hytuan@che.nthu.edu.tw; Fax: +886-3-571-5408; Tel: +886-3-572-3661

† Electronic supplementary information (ESI) available: Cycling life curve for GeO_2 nanoparticles at different electrolyte systems at 0.1C and 1C. See DOI: 10.1039/c6ra20171g

represent kinetics improvement related to rate capability for LIBs. Another strategy to ameliorate GeO_2 poor performance is size-controlled and architecture-design of the active material. Size and morphology of active material indeed play an important role in electrochemical performance for LIBs. Various nanostructures of GeO_2, such as nanotube,[31] nanoparticle,[32,33] 3-D porous nanostructure,[34] exhibit a high reversible capacity and capacity retention with slightly capacity fade, which implies the alleviation of stress from Li intercalation/de-intercalation to maintain electrode integrity. They also perform well in rate capability determined by the kinetics of electron conductivity and lithium diffusivity. On the basis of time constant τ, kinetics strongly depend on the diffusivity length ($\tau \approx L^2D^{-1}$). However, these methods used to synthesize GeO_2 nanostructures, such as thermal oxidation,[35,36] template-directed method,[37–39] and thermal evaporation,[40] usually need harsh experimental conditions or complicated manufacturing process, which not only produce unnecessary impurities harmful to environment but also increase the manufacturing cost. Those synthetic methods for GeO_2 might not be suited for industrial-scale production. Besides, GeO_2 nanomaterials were usually incorporated with carbon additives, such as carbon nanotube, graphene, 2-D matrix for assembling into LIBs. The batteries gain stable cycling life or increase specific capacity, but sacrifice the overall energy density due to the addition of extra volume and weight to electrode. Therefore, a suitable strategy is required to fabricate GeO_2 nanoparticles on the purpose of sustainability and scalability.

Herein, we report the synthesis of high quality hexabranched GeO_2 nanoparticles at room temperature with a nearly 100% yield *via* an optimized sol–gel process (reverse micelle). With well controlling the oil/water phase, surfactant/co-surfactant ratio and choosing the right germanium source, the well-defined GeO_2 nanoparticles can be obtained abundantly. In addition, as-prepared GeO_2 nanoparticles were used as anode materials for lithium ion batteries without any post-treatment. The electrochemical results demonstrate high capacity and quite stable capacity retention. Finally, coin type and pouch type full cells assembled with the GeO_2 as anode and Li(NiCoMn)O_2 as cathode are fabricated and evaluated. Pouch type full cells were utilized to power light-emitting-diodes (LEDs) over 120 bulbs with a large current (~650 mA).

Experimental

Material synthesis

Hexabranched GeO_2 nanoparticles were synthesized by a micro emulsion method in a nonionic reverse micelle system at ambient temperature.[41] The reverse micelle solution is prepared by well mixing 50 ml hexane (97.05%, Alfa Aesar), 47.4 g Triton-X-100 (Laboratory grade, Sigma Aldrich), 45 ml 1-hexanol (reagent, 98%, Sigma Aldrich), 18 ml pH = 1 hydrogen chloride (HCl) (37%, Sigma Aldrich) solution together first by closing the valve below the reactor, and the mixture is stirred for half an hour in the reactor at room temperature until the solution become transparent. Next, 4.2 g germanium ethoxide ($Ge(OEt)_4$) (99.995%, Alfa Aesar) was injected into the reactor for the further reaction. After about 5 minutes, the resulting solution became turbid under vigorous stirring for one hour at room temperature. White product powders weight in proximity of 1.2 g can be collected on a filter paper.

Characterization

To comprehend crystal structure of the product, X-ray diffraction with Cu Kα radiation operated at 40 kV and 20 mA was utilized. The morphology of GeO_2 was characterized by field emission scanning electron microscope (FE-SEM, Hitachi SU8010) operated at 10 kV accelerating voltage with working distances ranging between 10 to 20 mm and transmission electron microscope (TEM, JEOL JEM-2100F) equipped with an EDS spectrometer. X-ray photoelectron spectrometer (XPS, PHI Quantera SXM/Auger: AES 650) analysis was executed to figure out the reaction mechanism of GeO_2 nanoparticles with lithium metal. The XPS sample was prepared by dissembling GeO_2-based coin cell after 100 times charging/discharging test, and the electrode was dispersed in diethyl carbonate (DEC) solvent with ultrasonic treatment half an hour to remove residual electrolyte.

Electrochemical characterization

GeO_2 nanoparticles were well mixed with conductive material Super P carbon black and PAA binder in ethanol solvent at the weight ratio of 60 : 20 : 20 and then the homogeneous slurry were tape casted onto a copper foil by doctor-blade film coater. The electrodes were dried at 50 °C in vacuum oven to evaporate ethanol solvent and pressed densely for fear of material exfoliation by means of rolling machine. Before cell assembling in Ar-filled glove box, the weight of pure active material is accurately acquired utilizing a microbalance with 0.1 μg resolution (Sartorius SE2) for capacity calculation, giving typical mass loading of 0.6 mg cm^{-2} The coin-type half-cells (CR2032) were assembled with anode electrodes made of GeO_2 nanoparticles, Li metal cathode, and separator soaked in electrolyte. The electrolyte was 1 M $LiPF_6$ in fluoro-ethylene carbonate/diethyl carbonate (FEC/DEC) (3 : 7 vol%).

In the fabrication of coin-type and pouch-type full cells, the Li(NiCoMn)O_2 electrode with a loading mass of 21.12 mg cm^{-2} was to replace lithium metal as reference/counter electrode, and the anodes GeO_2 nanoparticles remained the same loading mass. For perfect full cell assembly, the electrochemical performance of the cathode Li(NiCoMn)O_2 was evaluated by half-cell measurement. The slurry for cathode electrode was prepared by mixing active materials (Li(NiCoMn)O_2, 94.5 wt%) with 3.5 wt% of Super-P and 2 wt% of PVDF (polyvinylidene fluoride) binder dispersed in NMP (*N*-methyl-2-pyrrolidone) solvent. From the Fig. S7,† the areal capacity for the cathode electrode was ~3.3 mA h cm^{-2} and the working potential of Li(NiCoMn)O_2 *vs.* Li was observed at 3.8 V. For pouch type full cell assembly, GeO_2 anode, membrane, and Li(NiCoMn)O_2 cathode were stacked orderly in the Al-laminated film after welding metallic strip terminal and then filled with electrolyte. For the sake of electrolyte soaking entirely, pouch type full cell were rest for half hour after cell sealing. All the electrochemical

performance of the GeO_2-based lithium ion batteries were evaluated using Maccor Series 4000 instruments.

Results and discussion

The micelle system for production of well-defined GeO_2 nanoparticles was conducted with the experimental setup represented in the Fig. 1. This process can be easily scaled up if sufficient precursor and suitable reactor volume are provided. Germanium ethoxide ($Ge(OEt)_4$) as organometallic precursor was directly injected into a flask containing hexane, 1-hexanol, Trion-X-100, and HCl solution, which serve as oil phase, surfactant, co-surfactant, and aqueous phase, respectively. ($Ge(OEt)_4$) dissolved in the nano-sized micelle capped with Triton-X-100 and 1-hexanol, and a perfectly mixing process lasted for 60 min. The white powder was obtained and the product GeO_2 weighted nearly 1.2 g in one batch shown in the Fig. 2(a). In a typical synthesis, the synthetic method could attain the product yield of approaching 100% under appropriate reaction operation. The large quantity GeO_2 nanoparticles obtained from the micelles system were directly used and suitable with current slurry coating technique for fabrication of lithium-ion batteries electrode.[42] To comprehend the growth mechanism of well-faceted GeO_2 nanoparticles, products formed with different reaction times were evaluated (Fig. S1†). With a reaction time 5 min, the product obtained was aggregated by irregularly shape nanoparticles, indicating a rapidly nucleation and multipoint growth mechanism for formation of GeO_2. After 10 min, GeO_2 particles have developed into hexabranched nanoparticles with more than 100 nm in length and large size distribution. GeO_2 nanoparticles transformed into hexagonally symmetrical shape probably related to its hexagonal crystal structure. After a half hour of reaction, the GeO_2 nanoparticles became more uniform in size as the same as those shown in Fig. 1.

The crystal structure of GeO_2 nanoparticles was investigated by X-ray diffraction analysis, as shown in Fig. 2(b). The XRD pattern perfectly matches the pure hexagonal phase structure of α-GeO_2 (JCPDS no. 36-1463 with unit cell constants $a = 4.985$ Å and $c = 5.648$ Å), and it is obvious that no impurity phase was observed. Further surface and morphology characterization of GeO_2 are provided by SEM images and the shape of product developed in this scale-up experiment design is hexabranched

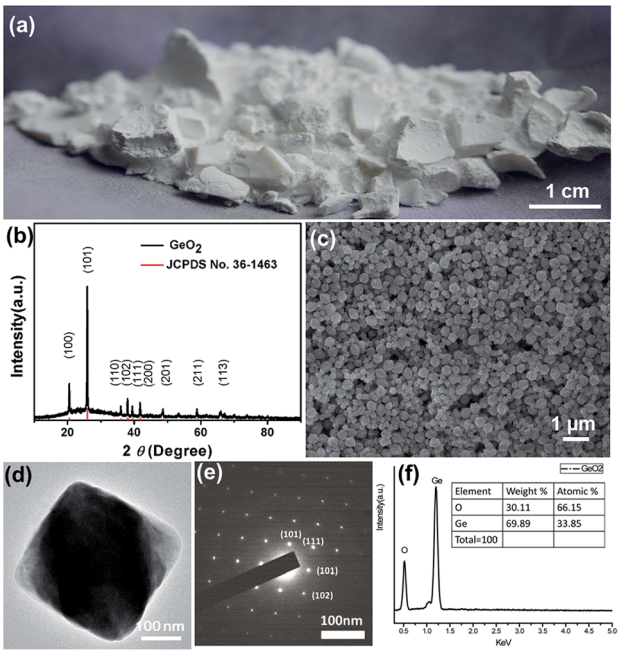

Fig. 2 (a) Photographical representation of the 1.2 grams GeO_2 powders synthesized by a microemulsion approach at room temperature. (b) XRD pattern, (c) SEM images, (d) TEM images, (e) SAED pattern, and (f) EDS analysis of hexabranched GeO_2 nanoparticles.

without transformation (Fig. 2(c)). The average length and width of the GeO_2 nanoparticles are determined to 200 ± 20 nm and 150 ± 25 nm based on statistics analysis over 500 nanoparticles measured from SEM images. TEM image and its corresponding selected area electron diffraction (SAED) of well-defined GeO_2 nanoparticle are given (Fig. 2(d) and (e)). Because of the inherent structural growth, the (101), (111) and (102) planes can be determined by diffraction perpendicular to the long axis. In addition, EDX analysis revealed the composition of GeO_2 nanoparticles showing exact atomic ratio shown in Fig. 2(f).

To evaluate the electrochemical performance of GeO_2 nanoparticles as anode material for LIBs, the product was assembled into coin type half-cell (CR2032) with Li metal as counter and reference electrode. First of all, the galvanostatic charging/discharging measurement was implemented at the current rate 0.1C (1C = 1.1 A g^{-1}) with working voltage window

Fig. 1 The illustration of experimental design of GeO_2 nanoparticles synthesized in microemulsion system at room temperature.

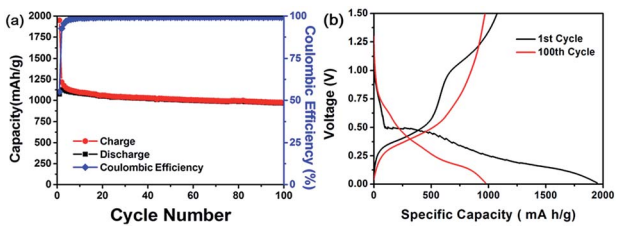

Fig. 3 (a) Charge/discharge cycle performance of GeO_2 anode at a 0.1C rate between 0.01 V and 1.5 V. (B) Voltage profiles of 1st and 100th cycle at a 0.1C rate.

of 0.01 V–1.5 V at room temperature. The cycling life curve in the Fig. 3(a) reveals that first charge and discharging capacity of the GeO_2 nanoparticles are 1948 mA h g^{-1} and 1074 mA h g^{-1}, respectively, corresponding to the coulombic efficiency of 55.1%. Presumably, the large irreversible capacity loss (874 mA h g^{-1}) in the first cycle is attributed to the formation of Li_2O, usually found in other metal oxide species such as silicon oxide.[43,44] According to the previous research,[23,45–47] it is believed that metal nanoparticles formed in delithiation process have catalytic property to decompose Li_2O, which improves the coulombic efficiency of initial charging/discharging test. After the following cycles, the average reversible capacity of GeO_2 nanoparticles was 1050 mA h g^{-1} with the excellent capacity retention of 87% based on the fifth cycle capacity (1105 mA h g^{-1}). The stability of cycling life curve represent the electrode prepared by hexabranched GeO_2 nanoparticles could tolerate the stress torture from huge variation during lithium intake and removal. Fig. 3(b) depicted the voltage profiles of the GeO_2 anode in the first cycle. During the charge process, the voltage decreases dramatically from the open circuit voltage to approximately 0.7 V, and the plateau region show up, and then the voltage further decreases slowly until around 0.15 V. In the discharge profile, the plateau can be clearly observed from 0.3 V to 0.6 V. To clearly understand the reaction mechanism of GeO_2 with lithium, differential capacity profiles shown in the Fig. 4(a) and (b) were derived from the voltage profiles of the first to 100th cycle in Fig. 3(a), and these peaks indicate various electrochemical reactions related to insertion/extraction of Li ions. Observed from the Fig. 4(a), there exist a distinct peak located near 0.5 V in the first charge cycle and vanished in the subsequent cycle, which probably present formation of SEI (solid electrolyte interface) layer and Li_2O in irreversibility.[33,48] At the following lithiation processes, small peak at approximately 0.13 V correspond to the Li–Ge alloying reaction. Correspondent Li–Ge de-alloying reaction is indexed to the small hump (0.35 V) in the delithiation process. Apparently, over several tens of times cycle test (Fig. 4(b)), the small peak around 0.37 V in the reduction sweep showed up, which is associated with formation of lithium-rich germanium alloys. Furthermore, the peaks at 0.62 V in reduction sweep and 0.7 V in oxidation sweep can be indicated to the redox reaction of germanium. However, the redox reaction reversibility is gradually decreasing, which may be a cause of capacity fading. These results are consistent with those reported research for cyclic voltammetry of GeO_2.[49,50] In reality, many electronic applications require high current operation. To confirm the feasibility of GeO_2 in practical application, high rate test of GeO_2-based batteries was executed. As shown in Fig. 5(a), current rate 1C with respect to 1100 mA h g^{-1} is employed and the discharge capacity is from 982 mA h g^{-1} in 2nd cycle to 856 mA h g^{-1} in 50th cycle with 87% capacity retention. Except 1C test, multi-rate with different operating current rates and its voltage profiles are depicted to examine the rate capability of GeO_2 anode (Fig. 5(b) and (c)). From Fig. 5(b), the plateau isn't obvious once cycled at high rate, which implies the difficulty in lithium insertion. At a high current density test, the lithium insertion into active material site is rate-determining step, which means the kinetic limitation hinder the further lithium ions react with GeO_2 nanoparticles.[51,52] The GeO_2 anode exhibits discharge capacities of 1250 mA h g^{-1}, 1100 mA h g^{-1}, 1000 mA h g^{-1}, 855 mA h g^{-1}, 590 mA h g^{-1}, 420 mA h g^{-1}, and 250 mA h g^{-1}, corresponding to the various current densities of 0.1C, 0.5C, 1C, 2C, 4C, 6C, and 8C, respectively shown in Fig. 5(c). Finally, the specific discharge capacity of about 1170 mA h g^{-1} is recovered fast when the rate is returned to 0.1C again after 35 cycles. The additional electrochemical performance of GeO_2 nanoparticles are provided in the ESI.† GeO_2-based batteries employ different composition electrolytes system showing diverse electrochemical performance. As shown in Fig. S1,† FEC/DMC electrolyte system possesses more stable capacity retention and high rate performance than that of EC/DMC electrolyte system, which is perhaps due to formation of good SEI layer on the electrode surface.[53–55]

To further understand the interfacial electrochemical behavior of GeO_2 electrodes, electrochemical impedance spectroscopy (EIS) analysis was performed at frequencies from 10 kHz to 10 mHz. From the Nyquist plots (Fig. 5(d)), the diameter of semicircle at high frequency region became small after charging/discharging test, which implies that transfer electron

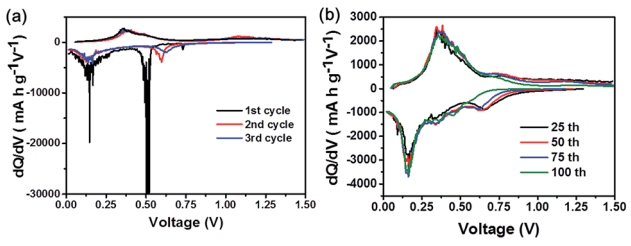

Fig. 4 Differential capacity profiles of the GeO_2 anode in the (a) 1st, 2nd, 3rd and following (b) 25th, 50th, 75th, 100th cycle derived from the galvanostatic charging/discharging curve at the rate of 0.1C.

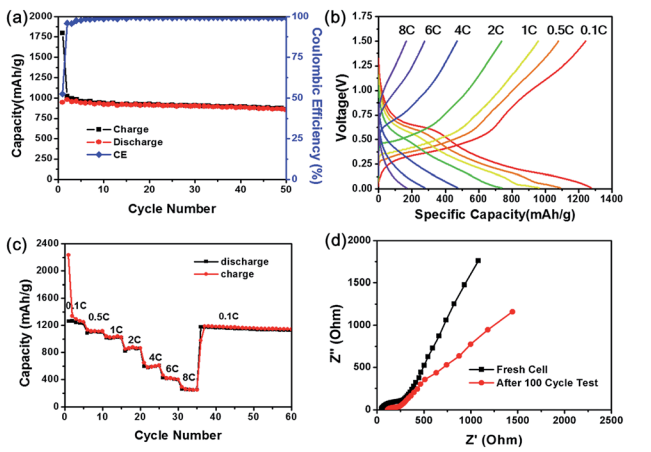

Fig. 5 Rate capability of GeO_2 nanoparticle anode. (a) Charge/discharge cycle performance of GeO_2 anode at a 1C rate between 0.01 V and 1.5 V. (b) Cycle performance of a 50-cycle test at rate range from 0.1C to 8C. (c) Voltage profiles of the performance in a 50-cycle test. (d) Nyquist plot for fresh/after 100 cycle test.

resistance reduces possibly due to the composition change of electrode such as formation of Li_2O matrix.[56–58] As for the inclined straight line at low frequency region, the slope of the line is relevant to lithium ion diffusivity which shows the difficulty for lithium ion immigration after 100 cycles.

In order to know the situation of composition and appearance of GeO_2 nanoparticles after electrochemical test, after 100th cycling in galvanostatic charge/discharge cycles at 0.1C rate was disassembled and cleaned with DEC solvent to remove residual byproducts. Fig. 6(a) demonstrates the intuitive evidences for before/after 100 cycling test in coin type cell, from the *ex situ* XPS measurement (Fig. 6(b)) of GeO_2 anode. It is obvious that the peak indicated (32.4 eV) corresponds to the Ge–O bonds. After cycling 100th cycles, the peak representing Ge–O bonding disappear, which is due to the full conversion of GeO_2 to form germanium nanoparticles and Li_2O. The single peak observed at 29.8 eV is well indicated to the elemental germanium. From XRD patterns shown in Fig. 6(c), there are two obvious peaks indexed to the (100) and (101) crystalline planes of GeO_2 nanoparticles with good crystallinity for fresh electrode. After cycled 100 times, the crystalline GeO_2 became amorphous, and showed no obvious peak from XRD pattern. Consequently, these evidences demonstrate that active material in the beginning is crystalline GeO_2 and finally turns to the amorphous germanium at the following cycles.

Volumetric capacity of active material is another essential consideration to evaluate the feasibility of the material applied to industrial development.[59–61] According to the characteristics of GeO_2 anode including gram-scale and great electrochemical properties analyzed in above experiments, the volumetric capacity of the GeO_2 is around 660 mA h cm^{-3} on the basis of compress density 0.6 g cm^{-3} (active material weight, electrode area, and the thickness of the GeO_2 electrode are 0.5 mg, 0.95 cm^2, and ~10 μm, respectively). This performance is higher than commercialized graphite anodes (370–500 mA h cm^{-3}).[62–64]

Coin type and pouch type full cell were fabricated combined with cathode ternary material $Li(NiCoMn)O_2$ to evaluate the feasibility of GeO_2 nanoparticles toward its application. Fig. 7(a) show the cycle performance of GeO_2 at rate of 0.1C in CR2032 coin type cells exhibited discharge capacities 1300 mA h g^{-1} in the first cycle between 2.5 V and 4.2 V and have a capacity of 950 mA h g^{-1} after 100 cycle. The subsequent slightly capacity fade is due to the unbalanced capacity ratio of cathode/anode and highly irreversible capacity of anodes. GeO_2-based coin type full cell also perform well at the rate of 1C with reversible capacity of 600 mA h g^{-1}. As for the pouch cell, the size of electrodes used in assembly is approximately 8 cm^2 × 5 cm^2, and the anode size is bigger to prevent Li-dendrite inside the cell. The mass loading of cathode and anode is the same as which is in CR2032 coin type cell. The total capacity and specific capacity are shown as Fig. 7(d). The capacity offered by the single pouch type battery at the rate 0.1C is 150 mA h (1878 mA h g^{-1}) in the first cycle, and the subsequent cycles show reversible capacity of approximately 70 mA h (800 mA h g^{-1}). To the best of our knowledge, it is the first time to incorporate the GeO_2 nanoparticles into the pouch-type cell fabrication process. A single battery is shown to power LED array over 120 bulbs which correspond to driving current 660 mA, a discharge rate 3C–4C, (Fig. 7(e)).

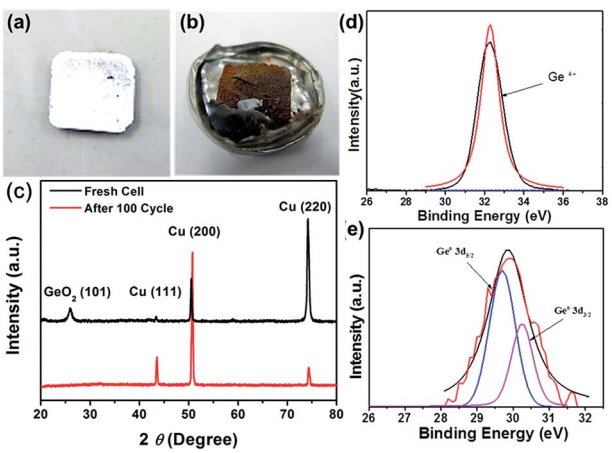

Fig. 6 (a, b) Photographs of GeO_2 anode color before/after 100th cycling intuitively (scale bar = 1 cm). (c) XRD pattern, (d, e) XPS analysis of GeO_2 anode before/after 100th cycling.

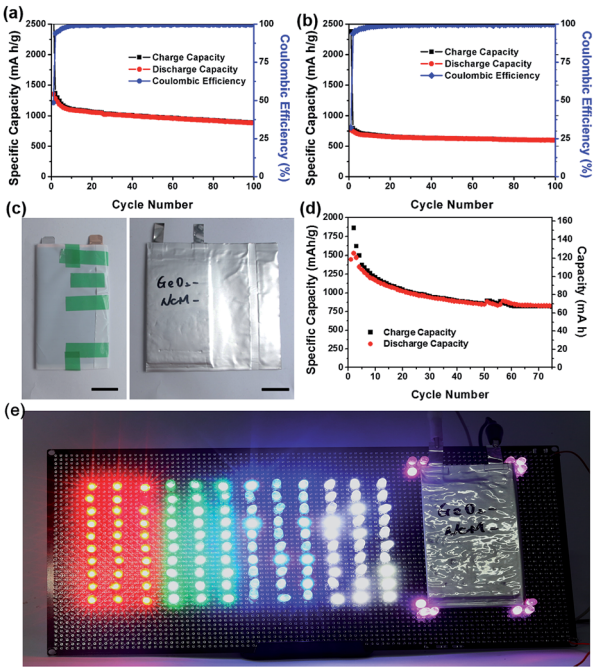

Fig. 7 (a) Cycle performance of the $Li(NiCoMn)O_2/GeO_2$ CR2032 coin type full cell at a 0.1C rate between 2.5 V and 4.2 V. (b) Cycle performance of the $Li(NiCoMn)O_2/GeO_2$ CR2032 coin type full cell at a 1C rate between 2.5 V and 4.2 V. (c) Photography of $Li(NiCoMn)O_2/GeO_2$ pouch type full cell. (d) Cycle performance (total capacity) of the $Li(NiCoMn)O_2/GeO_2$ pouch type full cell at a 0.1C rate between 2.5 V and 4.2 V. (e) Demonstration of pouch-type full cell to power LEDs array with a maximum current of 650 mA.

Conclusions

Nearly 100% yield of GeO_2 nanoparticles was prepared by a green synthesis method in reverse micelle system at room

temperature and exhibits superior electrochemical performance. As Li-ion batteries anode without any treatment, GeO_2 nanoparticles developed in this work exhibit excellent gravimetric capacity (1050 mA h g^{-1} at 0.1C rate), and a good rate capability over tens of cycles, and perform well in volumetric capacity (660 mA h cm^{-3}). Furthermore, coin type and pouch type full cells are successfully assembled with ternary cathode $Li(NiCoMn)O_2$ to power a wide range of electronic application devices. The utilization of GeO_2 as LIB anodes still have a challenging issue about low first coulombic efficiency induced by the irreversible process, which consume excess lithium ions to form Li_2O. In the future, we believe that strategies to address the limitation of coulombic efficiency, combined with the scalable nanoparticle synthesis, high electrochemical performance in gravimetric and volumetric capacity, makes GeO_2 a promising opportunity for the forthcoming low-cost and high energy density lithium-ion batteries.

Acknowledgements

We acknowledge the financial support by the Ministry of Science and Technology through the grants of NSC 102-2221-E-007-023-MY3, MOST 103-2221-E-007-089-MY3, MOST 103-2622-E-007-025, and MOST 102-2633-M-007-002.

Notes and references

1 V. Etacheri, R. Marom, R. Elazari, G. Salitra and D. Aurbach, *Energy Environ. Sci.*, 2011, **4**, 3243–3262.
2 P. Poizot, S. Laruelle, S. Grugeon, L. Dupont and J. M. Tarascon, *Nature*, 2000, **407**, 496–499.
3 J. M. Tarascon and M. Armand, *Nature*, 2001, **414**, 359–367.
4 M. Osiak, H. Geaney, E. Armstrong and C. O'Dwyer, *J. Mater. Chem. A*, 2014, **2**, 9433–9460.
5 F. W. Yuan, H. J. Yang and H. Y. Tuan, *ACS Nano*, 2012, **6**, 9932–9942.
6 P. R. Abel, K. C. Klavetter, K. Jarvis, A. Heller and C. B. Mullins, *J. Mater. Chem. A*, 2014, **2**, 19011–19018.
7 J. G. Ren, Q. H. Wu, H. Tang, G. Hong, W. J. Zhang and S. T. Lee, *J. Mater. Chem. A*, 2013, **1**, 1821–1826.
8 D. Li, C. Q. Feng, H. K. Liu and Z. P. Guo, *J. Mater. Chem. A*, 2015, **3**, 978–981.
9 T. Kennedy, E. Mullane, H. Geaney, M. Osiak, C. O'Dwyer and K. M. Ryan, *Nano Lett.*, 2014, **14**, 716–723.
10 F. W. Yuan and H. Y. Tuan, *Chem. Mater.*, 2014, **26**, 2172–2179.
11 C. N. R. Rao and A. K. Cheetham, *J. Mater. Chem.*, 2001, **11**, 2887–2894.
12 H. B. Wu, J. S. Chen, H. H. Hng and X. W. Lou, *Nanoscale*, 2012, **4**, 2526–2542.
13 M. Z. Ge, C. Y. Cao, J. Y. Huang, S. H. Li, Z. Chen, K. Q. Zhang, S. S. Al-Deyabd and Y. K. Lai, *J. Mater. Chem. A*, 2016, **4**, 6772–6801.
14 P. Roy and S. K. Srivastava, *J. Mater. Chem. A*, 2015, **3**, 2454–2484.
15 X. M. Lu, D. D. Fanfair, K. P. Johnston and B. A. Korgel, *J. Am. Chem. Soc.*, 2005, **127**, 15718–15719.
16 J. M. Buriak, *Chem. Rev.*, 2002, **102**, 1271–1308.
17 S. V. Patwardhan and S. J. Clarson, *Polymer*, 2005, **46**, 4474–4479.
18 A. R. Phani, D. Di Claudio, M. Passacantando and S. Santucci, *J. Non-Cryst. Solids*, 2007, **353**, 692–696.
19 H. Z. Li, L. Y. Yang, J. Liu, S. T. Li, L. B. Fang, Y. K. Lu, H. R. Yang, S. L. Liu and M. Lei, *J. Power Sources*, 2016, **324**, 780–787.
20 J. Liu, P. J. Lu, S. Liang, J. Liu, W. Wang, M. Lei, S. Tang and Q. Yang, *Nano Energy*, 2015, **12**, 709–724.
21 J. Liu, S. S. Tang, Y. K. Lu, G. M. Cai, S. Q. Liang, W. J. Wang and X. L. Chen, *Energy Environ. Sci.*, 2013, **6**, 2691–2697.
22 P. J. Lu, M. Lei and J. Liu, *CrystEngComm*, 2014, **16**, 6745–6755.
23 L. Mei, M. L. Mao, S. L. Chou, H. K. Liu, S. X. Dou, D. H. L. Ng and J. M. Ma, *J. Mater. Chem. A*, 2015, **3**, 21699–21705.
24 H. Y. Qiu, L. X. Zeng, T. B. Lan, X. K. Ding and M. D. Wei, *J. Mater. Chem. A*, 2015, **3**, 1619–1623.
25 J. S. Pena, I. Sandu, O. Joubert, F. S. Pascual, C. O. Arean and T. Brousse, *Electrochem. Solid-State Lett.*, 2004, **7**, A278–A281.
26 L. X. Zeng, X. X. Huang, X. Chen, C. Zheng, Q. R. Qian, Q. H. Chen and M. D. Wei, *ACS Appl. Mater. Interfaces*, 2016, **8**, 232–239.
27 A. Jahel, A. Darwiche, C. M. Ghimbeu, C. Vix-Guterl and L. Monconduit, *J. Power Sources*, 2014, **269**, 755–759.
28 S. Yoon, S. H. Jung, K. N. Jung, S. G. Woo, W. Cho, Y. N. Jo and K. Y. Cho, *Electrochim. Acta*, 2016, **188**, 120–125.
29 D. T. Ngo, H. T. T. Le, R. S. Kalubarme, J. Y. Lee, C. N. Park and C. J. Park, *J. Mater. Chem. A*, 2015, **3**, 21722–21732.
30 J. Hwang, C. Jo, M. G. Kim, J. Chun, E. Lim, S. Kim, S. Jeong, Y. Kim and J. Lee, *ACS Nano*, 2015, **9**, 5299–5309.
31 Y. Chen, C. L. Yan and O. G. Schmidt, *Adv. Energy Mater.*, 2013, **3**, 1269–1274.
32 Y. Son, M. Park, Y. Son, J. S. Lee, J. H. Jang, Y. Kim and J. Cho, *Nano Lett.*, 2014, **14**, 1005–1010.
33 Y. M. Lin, K. C. Klavetter, A. Heller and C. B. Mullins, *J. Phys. Chem. Lett.*, 2013, **4**, 999–1004.
34 X. L. Wang, W. Q. Han, H. Y. Chen, J. M. Bai, T. A. Tyson, X. Q. Yu, X. J. Wang and X. Q. Yang, *J. Am. Chem. Soc.*, 2011, **133**, 20692–20695.
35 S. L. Shinde and K. K. Nanda, *CrystEngComm*, 2013, **15**, 1043–1046.
36 M. Gunji, S. V. Thombare, S. Hu and P. C. McIntyre, *Nanotechnology*, 2012, **23**, 385603.
37 Y. J. Zhang, J. Zhu, Q. Zhang, Y. J. Yan, N. L. Wang and X. Z. Zhang, *Chem. Phys. Lett.*, 2000, **317**, 504–509.
38 Q. Y. Lu, F. Gao, Y. Q. Li, Y. M. Zhou and D. Y. Zhao, *Microporous Mesoporous Mater.*, 2002, **56**, 219–225.
39 X. D. Zou, T. Conradsson, M. Klingstedt, M. S. Dadachov and M. O'Keeffe, *Nature*, 2005, **437**, 716–719.
40 Z. Jiang, T. Xie, G. Z. Wang, X. Y. Yuan, C. H. Ye, W. P. Cai, G. W. Meng, G. H. Li and L. D. Zhang, *Mater. Lett.*, 2005, **59**, 416–419.
41 Y. W. Chiu and M. H. Huang, *J. Phys. Chem. C*, 2009, **113**, 6056–6060.
42 N. Liu, H. Wu, M. T. McDowell, Y. Yao, C. M. Wang and Y. Cui, *Nano Lett.*, 2012, **12**, 3315–3321.

43 Y. R. Wang, W. Zhou, L. P. Zhang, G. S. Song and S. Q. Cheng, *RSC Adv.*, 2015, **5**, 63012–63016.
44 N. Yan, F. Wang, H. Zhong, Y. Li, Y. Wang, L. Hu and Q. W. Chen, *Sci. Rep.*, 2013, **3**, 1568.
45 K. H. Seng, M. H. Park, Z. P. Guo, H. K. Liu and J. Cho, *Nano Lett.*, 2013, **13**, 1230–1236.
46 C. H. Kim, Y. S. Jung, K. T. Lee, J. H. Ku and S. M. Oh, *Electrochim. Acta*, 2009, **54**, 4371–4377.
47 Y. G. Zhu, Y. Wang, Z. J. Han, Y. Shi, J. I. Wong, Z. X. Huang, K. Ostrikov and H. Y. Yang, *Nanoscale*, 2014, **6**, 15020–15028.
48 D. T. Ngo, R. S. Kalubarme, H. T. T. Le, C. N. Park and C. J. Park, *Nanoscale*, 2015, **7**, 2552–2560.
49 D. T. Ngo, R. S. Kalubarme, M. G. Chourashiya, C. N. Park and C. J. Park, *Electrochim. Acta*, 2014, **116**, 203–209.
50 H. P. Jia, R. Kloepsch, X. He, J. P. Badillo, M. Winter and T. Placke, *J. Mater. Chem. A*, 2014, **2**, 17545–17550.
51 Y. G. Li, B. Tan and Y. Y. Wu, *Nano Lett.*, 2008, **8**, 265–270.
52 J. R. Dahn, T. Zheng, Y. H. Liu and J. S. Xue, *Science*, 1995, **270**, 590–593.
53 A. M. Chockla, K. C. Klavetter, C. B. Mullins and B. A. Korgel, *ACS Appl. Mater. Interfaces*, 2012, **4**, 4658–4664.
54 S. S. Zhang, *J. Power Sources*, 2006, **162**, 1379–1394.
55 Y. M. Lin, K. C. Klavetter, P. R. Abel, N. C. Davy, J. L. Snider, A. Heller and C. B. Mullins, *Chem. Commun.*, 2012, **48**, 7268–7270.
56 M. Itagaki, K. Honda, Y. Hoshi and I. Shitanda, *J. Electroanal. Chem.*, 2015, **737**, 78–84.
57 Y. W. Li, J. H. Yao, E. Uchaker, J. W. Yang, Y. X. Huang, M. Zhang and G. Z. Cao, *Adv. Energy Mater.*, 2013, **3**, 1171–1175.
58 B. Luo, Y. Fang, B. Wang, J. S. Zhou, H. H. Song and L. J. Zhi, *Energy Environ. Sci.*, 2012, **5**, 5226–5230.
59 X. H. Wang, L. N. Sun, R. A. Susantyoko, Y. Fan and Q. Zhang, *Nano Energy*, 2014, **8**, 71–77.
60 H. L. Cao, X. F. Zhou, W. Deng and Z. P. Liu, *J. Mater. Chem. A*, 2016, **4**, 6021–6028.
61 K. C. Klavetter, J. P. de Souza, A. Heller and C. B. Mullins, *J. Mater. Chem. A*, 2015, **3**, 5829–5834.
62 S. Jeong, J. P. Lee, M. Ko, G. Kim, S. Park and J. Cho, *Nano Lett.*, 2013, **13**, 3403–3407.
63 B. Wang, X. L. Li, T. F. Qiu, B. Luo, J. Ning, J. Li, X. F. Zhang, M. H. Liang and L. J. Zhi, *Nano Lett.*, 2013, **13**, 5578–5584.
64 X. P. Wang, L. X. Lv, Z. H. Cheng, J. A. Gao, L. Y. Dong, C. G. Hu and L. T. Qu, *Adv. Energy Mater.*, 2016, **6**, 1502100.